Journal Pre-proof

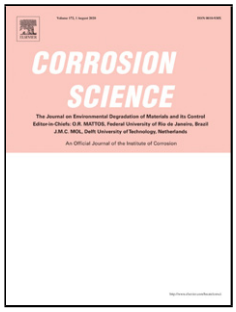

Facile fabrication of SnO_2 modified TiO_2 nanorods film for efficient photocathodic protection of 304 stainless steel under simulated solar light

Zhang Juantao, Yang Hualong, Wang Yuan, Cui Xiaohu, Wen Zhang, Fan Lei, Liu Yunpeng, Feng Jiangtao

PII: S0010-938X(20)30830-1

DOI: https://doi.org/10.1016/j.corsci.2020.108927

Reference: CS 108927

To appear in: *Corrosion Science*

Received Date: 7 April 2020

Revised Date: 12 July 2020

Accepted Date: 2 August 2020

Please cite this article as: Juantao Z, Hualong Y, Yuan W, Xiaohu C, Zhang W, Lei F, Yunpeng L, Jiangtao F, Facile fabrication of SnO_2 modified TiO_2 nanorods film for efficient photocathodic protection of 304 stainless steel under simulated solar light, *Corrosion Science* (2020), doi: https://doi.org/10.1016/j.corsci.2020.108927

Facile fabrication of SnO_2 modified TiO_2 nanorods film for efficient photocathodic protection of 304 stainless steel under simulated solar light

Zhang Juantao [a], Yang Hualong [b], Wang Yuan [a], Cui Xiaohu [b], Wen Zhang [b], Fan Lei [a, *], Liu Yunpeng [c, **] and Feng Jiangtao [c, ***]

a NPC Tubular Goods Research Institute, State Key Laboratory for Performance and Structure Safety of Petroleum Tubular Goods and Equipment Materials, Xi'an, Shaanxi 710077, China

b Petro China Traim Oilfield Company, Korla, 841000, China

c Department of Environmental Science & Engineering, Xi'an Jiaotong University, Xi'an, 710049, China.

Corresponding authors:

Fan Lei: damifan198802@163.com

Liu Yunpeng: liuyunpeng1994@stu.xjtu.edu.cn

Feng Jiangtao: fjtes@xjtu.edu.cn

Graphical abstract

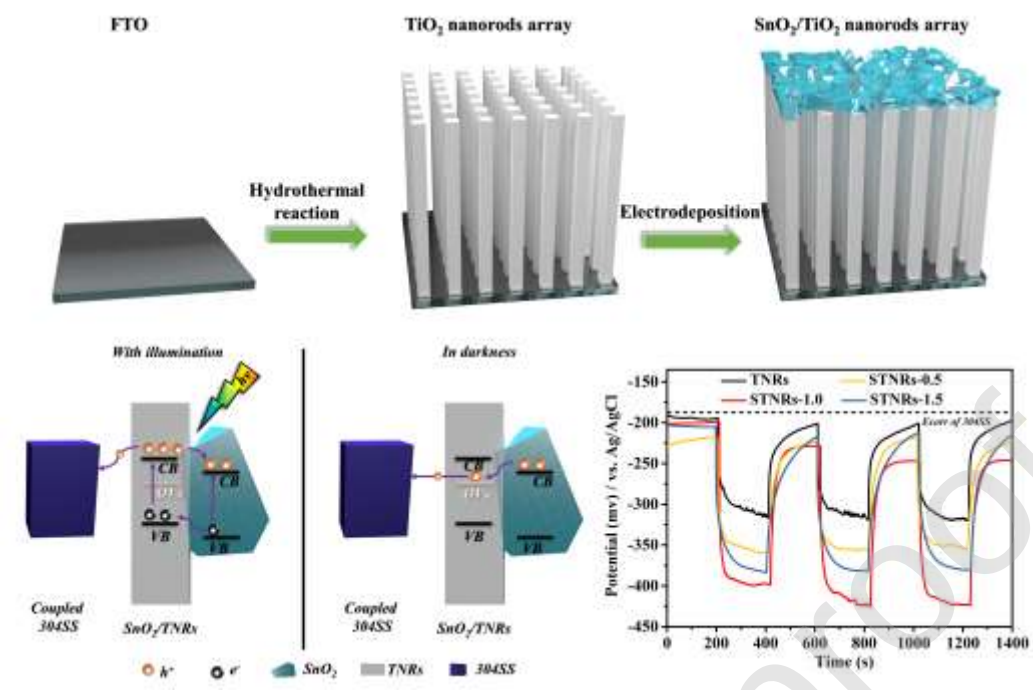

Highlights

- SnO_2/TiO_2 nanorods (TNRs) films are successfully synthesized.
- SnO_2/TNRs film exhibits superior light absorption ability.
- SnO_2/TNRs film displays excellent cathodic protection performance under simulated solar light.
- Under dark condition, SnO_2/TNRs film can provide continuous protection for the steel.

Abstract

SnO_2/TiO_2 nanorods (TNRs) composite film was successfully fabricated. The results showed that the SnO_2 nanoparticles were deposited onto the surface of the TNRs film, and this composite film exhibited excellent light absorption ability. Meanwhile, the SnO_2/TNRs composite film exhibited the superior photoelectrochemical performance. With white light illumination, this composite film made the potential of the coupled 304 stainless steel (304SS) in a 0.5 $mol \cdot L^{-1}$ NaCl solution drop by 240 mV, exhibiting more efficient photocathodic protection (PCP) effect. What's more, it could provide delay protection for the steel in darkness attributing to the "electron pool" effect of SnO_2.

Keywords: TiO_2 nanorods array, SnO_2, 304 stainless steel, photocathodic protection

1. Introduction

304SS is widely used as engineering steel in industrial production due to its outstanding anti-corrosion property. Nevertheless, pitting and crevice corrosion on the metals are barely to be avoided in the presence of Cl^- [1-3]. So far, many anti-corrosion technologies have been developed, such as anti-corrosion coatings, corrosion inhibitors, electrochemical protection, etc [4, 5]. These traditional protection technologies are limited because of the consumption of material and energy, and the environmental

pollution. On behalf of green steel-protection methods, the PCP is commonly considered as the one of the most effective technology [6]. When the photoanode is irradiated, the photoexcited electrons are immigrated to the connected steel, and the surface potential of the protected steel shifted negatively below its corrosion potential, resulting in the cathodic protection effect for metals [7].

TiO_2 has attracted many attentions in field of photocatalysis, owing to its low cost, low toxicity and large specific surface area properties. Compared with traditional TiO_2 particles and TiO_2 nanotubes (TNTs) array, TNRs array has been extensively exploited in pollution degradation, hydrogen production and solar cells due to one-dimensional (1D) electron transmission shortcut and excellent electronic mobility [8]. However, TNRs still suffers the inherent flaws of TiO_2, namely, the wide band gap (3.1 eV) of rutile TiO_2 limits its PCP application only in the UV region and decrease the utilization ratio of solar light [9]. Meanwhile, the rapid recombination of photogenerated electrone/hole (e^-/h^+) pairs will happen after cutting off the light, resulting in the lose effectiveness of the cathodic protection in darkness [10]. Thus, in order to enhance the PCP performance, it is necessary to sensitize TNRs as a visible light absorber. At present, the combination of TNRs and narrow band-gap semiconductors (such as Bi_2S_3, WO_3, CdSe, etc.) have been proved to be effective methods to hinder with these problems [11].

SnO_2, a kind of stable and nontoxic n-type (3.5 eV) semiconductor, has be used to combine with TiO_2 to form photoanode in some PCP researches [12]. The stagger band

structure between SnO_2 and TiO_2, benefits the separation of the e^-/h^+ pairs to enhance photoelectric performance. In addition, since the conduction band (CB) of TiO_2 is more positive than that of SnO_2, SnO_2 can serve as an "electron pool" to storage e^- in the binary photoanode material, to ultimately provide delay protection for the coupled steel in darkness [13]. Hu et al. have synthesized SnO_2 nanoparticles modified TiO_2 nanotube films, and provided an effective cathodic protection for 403 stainless steel [9]. Zhang et al. have fabricated nanoflower like SnO_2-TiO_2 nanotubes photoanode, and the delay protection for 304SS was achieved in darkness [13]. However, as the excellent succedaneous materials of TNTs film, there have been no reports on the PCP efficiency effects of the SnO_2/TNRs composite for 304SS.

Therefore, in this work, the main objective is to synthesize the SnO_2/TNRs film via hydrothermal treatment and electrodeposition method on the conductive fluorine-doped tin oxide (FTO) substrates, to achieve excellent PCP efficiency for 304SS. Meanwhile, their photoelectrochemical properties and PCP mechanism for 304SS were also proposed.

2. Materials and methods

2.1 Chemicals

Hydrochloric acid (HCl), nitric acid (HNO_3), stannic chloride ($SnCl_2$), sodium hydroxide (NaOH), sodium chloride (NaCl), sodium sulphide (Na_2S), sodium nitrate ($NaNO_3$) and titanium butoxide ($C_{16}H_{36}O_4Ti$) were all purchased from Sinopharm

Chemical Regent Co. Ltd, (Shanghai, China). All the chemicals were analytical reagent without any purification and distilled water (DW) was used in the preparation of all solutions.

FTO glass (7 $\Omega \cdot cm^{-2}$, 2.2 mm-thick) was bought from Guluo Glass Co. Ltd, (Luoyang, China). Before using of the testes, the FTO glasses were cleaned ultrasonically by DW, followed by acetone and alcohol for 30 min each. In the end, those structures were air-dried in ambient condition.

2.2 Synthesis of SnO_2/TNRs composite films

2.2.1 Preparation of TNRs film

The TNRs array film was fabricated on FTO substrate by the traditional hydrothermal reaction following these steps. In the first place, 60 mL HCl aqueous solution (6 $mol \cdot L^{-1}$) injected with 1.0 mL $C_{16}H_{36}O_4Ti$, was poured into a 100 mL Teflon-lined stainless-steel autoclave. Then a sheet of FTO structure was put at an angle against the wall of the above autoclave with the conducting side facing down, and being heated at 150 °C in an electric oven (for 10 h). Finally, the film was washed with DW, and placed in a muffle furnace at 500 °C in air (for 2 h).

2.2.2 Preparation of SnO_2/TNRs composite film

SnO_2/TNRs composite films were prepared in a traditional three-electrode system. The work electrode (WE), the reference electrode (RE) and the counter electrode (CE) are corresponded to the TNRs film, Ag/AgCl electrode and Pt foil, respectively. The electrodeposition solution comprised 25 $mmol \cdot L^{-1}$ $SnCl_2$ and 50 $mmol \cdot L^{-1}$ HNO_3. The

electrodeposition method was carried out potentiostatically (CHI660D, Shanghai Chinstruments co., Ltd, China) at 0.5 V under room temperature condition. After thoroughly rinsed with deionized water and dried in a vacuum drying oven at 50 °C (for 12 h), these as-deposited composite films were annealed at 450 °C under air atmosphere (for 2 h). Fig. 1 display the schematic illustration for preparing these composites. To compare the PCP performances of the SnO_2/TNRs composite films with different deposition time, the SnO_2/TNRs composite films with different electrodeposition time (0.5, 1 and 1.5 h) was synthesized, denoting as SnO_2/TNRs-0.5 h SnO_2/TNRs-1 h and SnO_2/TNRs-1.5 h, respectively.

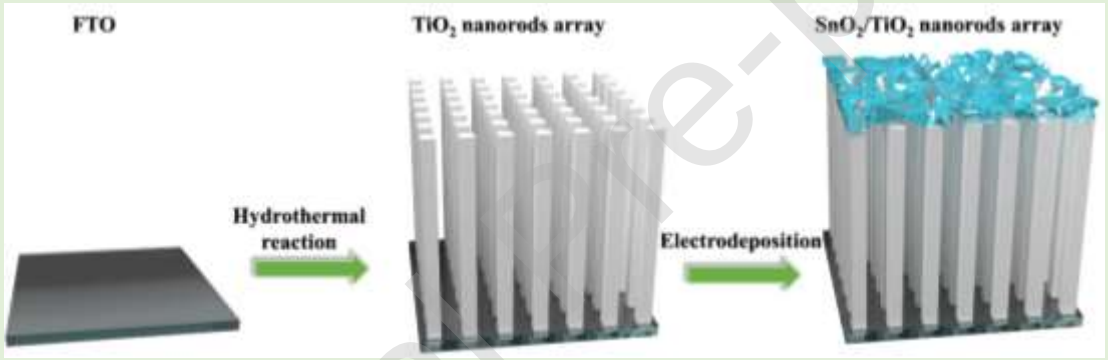

Fig. 1. Schematic illustration of the construction process of SnO_2/TiO_2 nanorods array composite.

2.3 Characterizations

All the as-prepared samples were characterized by scanning electron microscope (SEM Zeiss Gemini SEM 500, Germany), X-ray diffraction instrument (Bruker D8 ADVANCE, Germany), Raman spectra (LabRAM HR Evolution with an excitation of 325 nm laser light, France), X-ray photoelectron spectroscopy (XPS, Thermo Scientific EscaLab 250Xi., USA), UV-vis diffuse reflectance absorption spectra (DRS, PE

Lambda950, USA). The photoluminescence (PL) spectra were measured using an Edinburgh FLS9 luminescence spectrofluophotometer with a Xe lamp presenting an excitation light of 340 nm. The time resolved photoluminescence (TRPL) was also studied on a FLS9 series of fluorescence spectrometers.

2.4 Photoelectrochemical tests

In the photoelectrochemical experiments, the test rig consisted of a corrosion cell (3.5 wt% NaCl solution) and a photoelectrode cell (0.1 mol·L^{-1} Na_2S + 0.2 mol·L^{-1} NaOH mixed solution), and the two cells were connected by a salt bridge (saturated KCl in agar gel). In the corrosion cell, the 304SS electrode, Ag/AgCl electrode and Pt foil were connected to WE, RE and CE poles of the CHI660D electrochemical workstation, respectively, and the as-prepared photoelectrode as the photoanode was immersed in photoelectrochemical cell, which was coupled with the steel electrode via a copper wire, as described previously [3]. The photoanodes with an effective irradiation area of 1 cm^2 were radiated by a 500 W Xenon arc lamp (CHF-XM-500W, Beijing Changtuo technology Co., Ltd. Beijing, China) coupled with an AM 1.5 G filter calibrated to 100 mW·cm^{-2}. The scanning rates of open circuit potentials (OCP) and Tafel curves were 1 mV/s. Meanwhile, no bias voltage was applied in the test of photocurrent density of the photoelectrode. The Tafel result was fitted to calculate the corrosion potential (E_{corr}) and the corrosion current density (I_{corr}). The efficient area of 304SS was 1 cm^2, which was ground with 2000-mesh abrasive paper and rinsed with acetone.

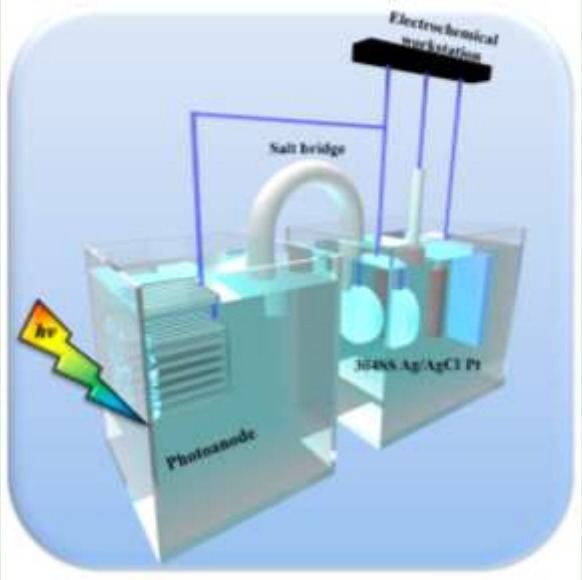

Fig. 2. Schematic of photoelectrochemical test device

3 Results and discussion

3.1 Structural characteristics

The structural information was provided by their Raman spectra and XRD patterns. As displayed in Fig. 3a, three strong characteristic Raman peaks (the curve of TNRs) were found to located at 230, 446 and 610 cm^{-1}, ascribed to the B_{1g}, E_g, A_{1g} modes of rutile TiO_2, respectively [14]. Moreover, any the characteristic peaks of anatase TiO_2, cannot be observed, indicating pure rutile phase was obtained after hydrothermal treatment. In the curve of STNRs-1.0, these characteristic peaks of SnO_2 were overlapped by the rutile TiO_2 signal for this composite film, so there is no difference between TNRs and STNRs-1.0. Furthermore, to confirm the composition of the STNRs-1.0 film, the XRD results of the TNRs and STNRs-1.0 were displayed in Fig. 3b. The diffraction peaks of the TNRs at 27.5°, 36.1°, 39.3°, 41.3°, 54.5° 62.9° and 69.8°correspond well to the (1 1 0), (1 0 1), (2 0 0), (1 1 1), (2 1 1), (0 0 2) and (1 1 2)

planes of rutile TiO_2 (JCPDS card no: 65-0912), respectively, which is consistent with the above Raman result [15]. After the electrodeposition of SnO_2 on the surface of TNRs film, the XRD curve of the STNRs-1.0 exhibits new diffraction peaks at 33.7°, 61.6° and 65.5°, which matches well with the characteristic XRD peaks ((1 1 0), (3 1 0) and (3 0 1)) of cassiterite SnO_2 (JCPDS card no: 41-1445) [16]. The XRD result demonstrates the successful deposition of SnO_2 on the surface of TNRs film.

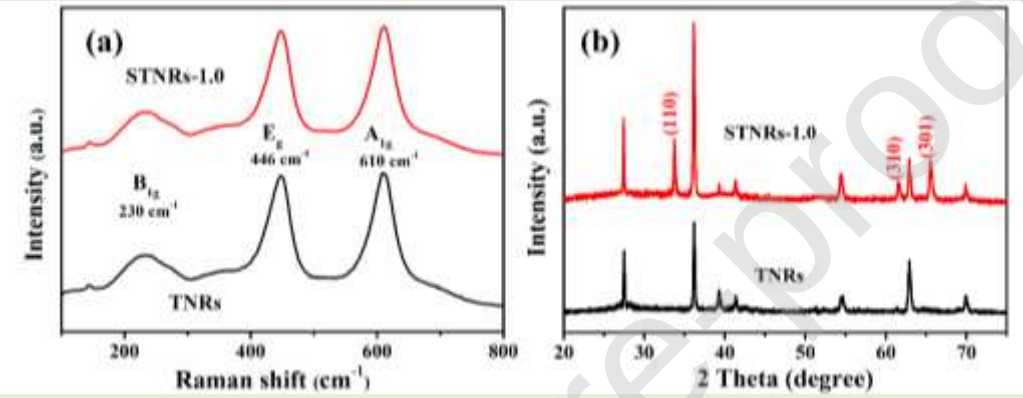

Fig. 3. The Raman spectra (a) and the XRD patterns (b) for the TNRs and STNRs-1.0.

Fig. 4 displays the SEM images with two different magnifications of TNRs film before and after SnO_2 loading. From the images of TNRs (Fig. 4a and b), the TNRs grew uniformly and densely on the surface of FTO glass, and the mean diameter of nanorods is about 150 nm. After electrodeposition treatment, there are amount of SnO_2 nanoparticles on the surface of TNRs film as shown in Fig. 4c. Moreover, the rod-like structure of TNRs maintains good property during the electrodeposition process (Fig. 4d). This result also indicates that the SnO_2 nanoparticles are successfully loaded on the TNRs film.

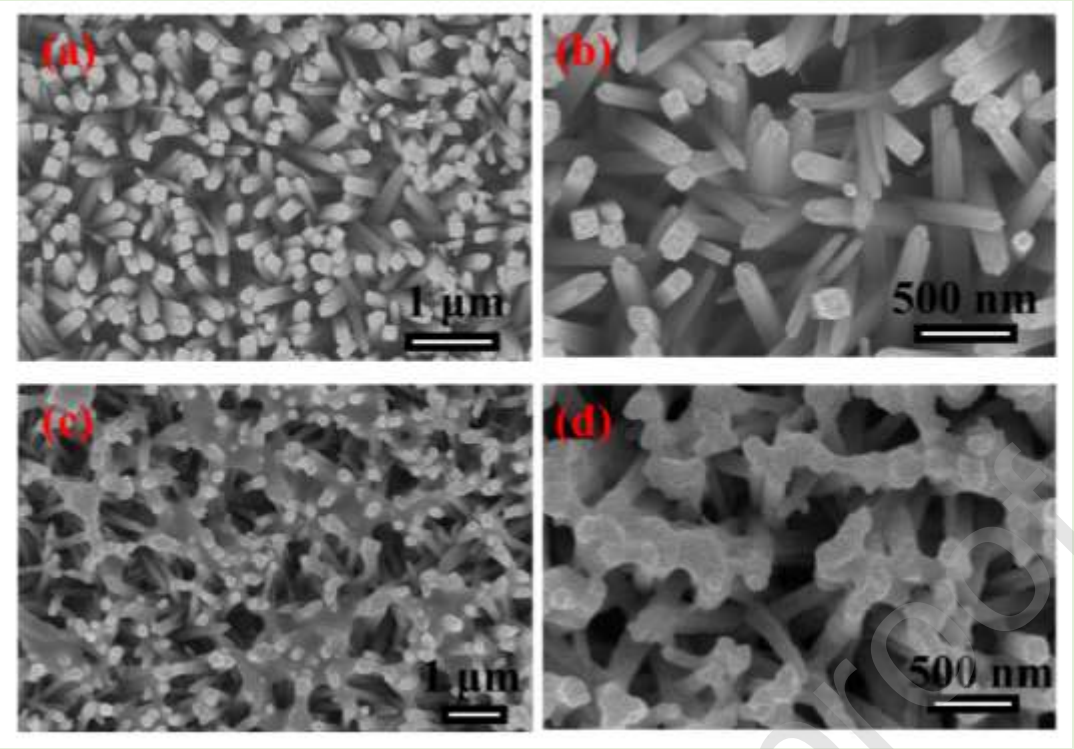

Fig. 4. SEM images of the TNRs (a and b) and STNRs-1.0 (c and d).

To further confirm the chemical compositions and elemental chemical statuses of the composite film, the as-synthesized STNRs-1.0 film was characterized by XPS, and the result is displayed in Fig. 5a-d. From the survey spectra shown in Fig. 5a, the Ti, Sn and O were present in the sample, and the C 1s peak in the figure is due to the surface pollution of C. High resolution XPS spectra for Sn 3d, O 1s and Ti 2p are displayed in Fig. 5b, c and d, respectively. The two peaks at 495.6 and 487.2 eV are ascribed to Sn $3d_{3/2}$ and Sn $3d_{5/2}$, respectively (Fig. 5b), implying that the main valence state of Sn in this sample is +4 [17]. As shown in Fig. 5c, binding energies at 530.4 eV and 531.8 eV, are corresponding to the contribution of lattice oxygen in TiO_2 and SnO_2 crystal lattice, and surficial hydroxyl groups (O-H), respectively [18, 19]. As shown in the XPS comparison curves of Ti 2p of TNRs and STNRs-1.0 (Fig. 5d), the binding energies at

463.9 eV and 458.2 eV of TNRs are ascribed to Ti $2p_{1/2}$ and Ti $2p_{3/2}$, respectively [20]. Compared with the previous reports [21], both of the Ti 2p peaks of the TNRs slightly shifted to the lower banding energy, which is ascribed to the destroy of Ti-O-Ti linkages of the TiO_6 octahedra in strong acid solutions, generating a small amount of oxygen vacancies (OVs) in the synthesis process of nanorods [22]. However, the content of OVs is not sufficient to impact the pure rutile phase of TNRs, according to the results of Raman and XRD spectra. After electrodeposition of SnO_2, all the Ti 2p peaks of the STNRs-1.0 films shifted negatively, indicating the interaction between TiO_2 and SnO_2. With the formation of heterojunction, the redistribution of valence electrons between TiO_2 and SnO_2 occurs [23], and the positive shift of Ti 2p indicates that the transfer tendency from SnO_2 to TiO_2.

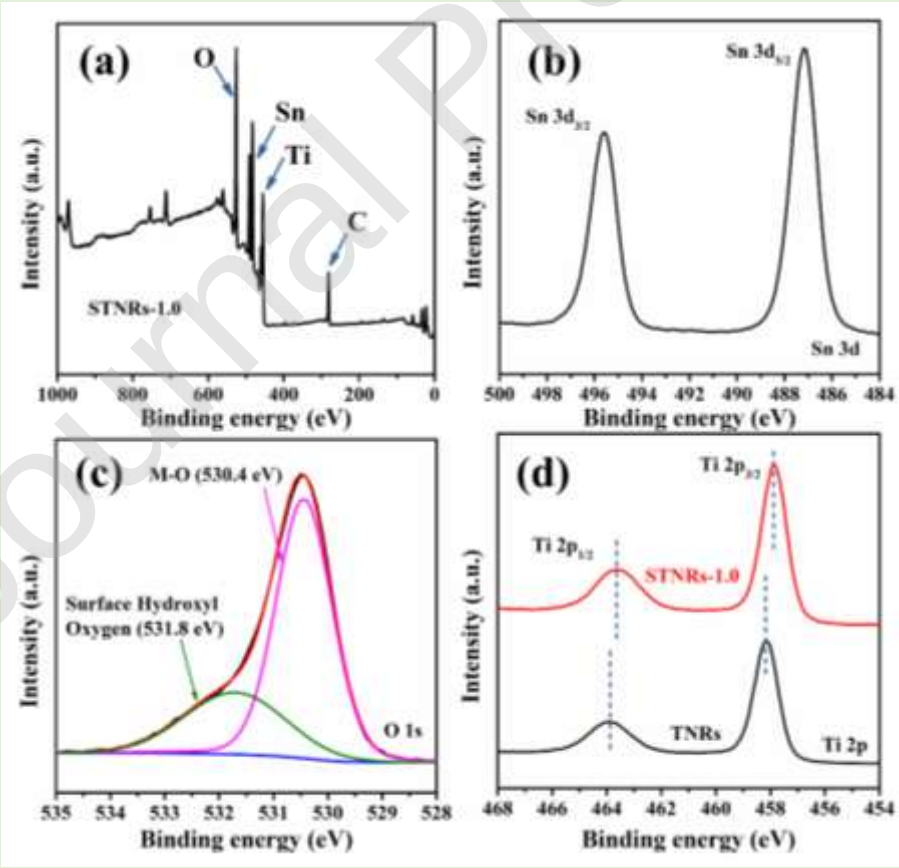

Fig. 5. Full scan survey XPS spectrum (a) and high-resolution spectra of (b) Sn 3d and (c) O 1s of STNRs-1.0 composite film, and the XPS comparison spectrum of Ti 2p (d) of TNRs and STNRs-1.0 films.

UV-Vis DRS was employed to study the optical properties of TNRs and SnO_2/TNRs films. As displayed in Fig. 6, the TNRs shows a typical absorption band-edge at about 390 nm, which agrees well with the band gap of rutile TiO_2 (E_g =3.10 eV) [3, 24]. After deposition of SnO_2, the as-prepared STNRs-1.0 composite shows much stronger absorption ability to the UV light, and slight red-shift of the absorption edge to the longer wavenumber region compared with the pure TNRs. The measured band-gap value of STNRs-1.0 composite is narrowed to be about 3.06 eV. This result demonstrates that the combination of TNRs and SnO_2 not only improve the solar-energy utilization efficiency of this photoanode, but also efficiently suppress the bulk recombination and surface recombination of the e^-/h^+ pairs, and finally promote its PCP properties for 304SS. Meanwhile, SnO_2 nanoparticles cannot absorb visible light due to its relatively wide band gap [25], resulting in the very slight optical absorption red-shift of STNRs-1.0 composites.

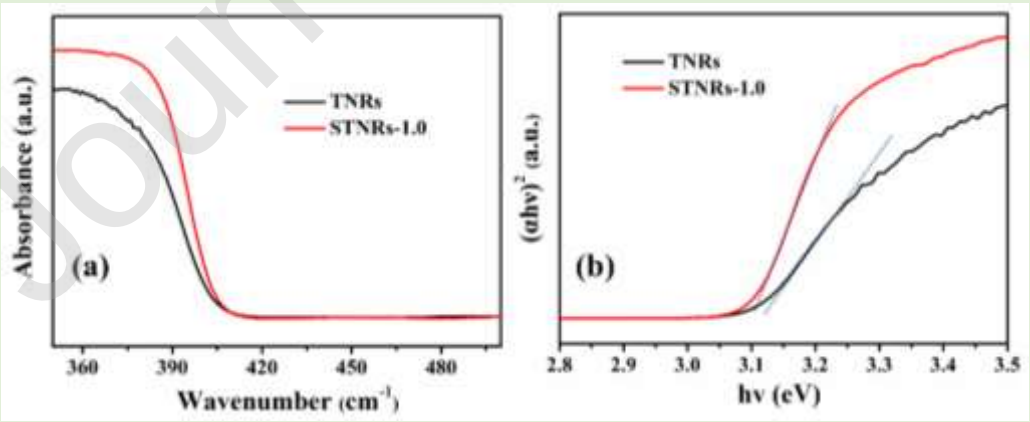

Fig. 6. UV-vis absorption spectra (a) and the plots of $(\alpha hv)^2$ versus hv (b) for the TNRs and STNRs-1.0 films.

In order to study the influence of the SnO_2 nanoparticles, PL emission spectrum and TRPL spectrum measurements were applied to reveal the migration, transfer and recombination processes of the e^-/h^+ pairs in the interface between SnO_2 and TNRs. As shown in Fig. 7a, the main emission peak is located at 435 nm for the pure TNRs, which can be contributed to the band-to-band recombination process of the e^-/h^+ pairs [26]. The higher PL intensity, the faster recombination rate of photocarriers. The PL peak intensity of the STNRs-1.0 was much lower for comparison with that of the pure TNRs, implying that the separation efficiency of the e^-/h^+ pairs in the composite film has been enhanced because of the deposition of SnO_2. For more insights into the photogenerated charges, TRPL analysis was displayed in Fig. 7b, and the lifetime of STNRs-1.0 (8.30 ns) is higher than that of pure TNRs (5.34 ns), indicating rapid charge immigration between SnO_2 and TNRs. These results demonstrated that the formation of built-in electric field in the interface can efficiently improve the transfer of photo-induced electrons and simultaneously hindered the recombination of the e^-/h^+ pairs.

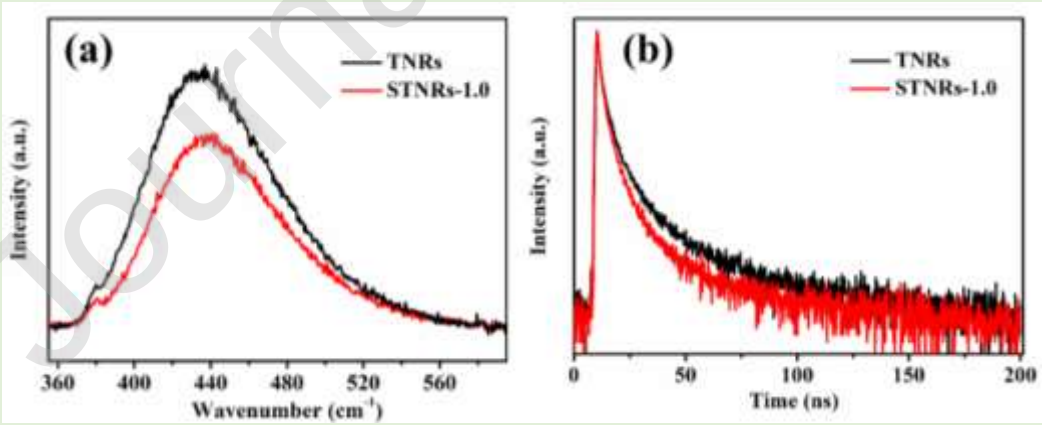

Fig. 7. PL emission spectra (a) and TRPL spectra (b) of TNRs and STNRs-1.0 composite films.

3.2 Photoelectrochemical properties of TNRs and SnO_2/TNRs film

The transfer of photoinduced electrons play an important role in PCP process, so it's essential for assessing the PCP efficiency of a photoanode to investigate the photocurrent density [27]. Fig. 8a shows the photocurrent density of the TNRs, and STNRs-0.5, STNRs-1.0 and STNRs-1.5 films connected with metal with intermittent white light irradiation. Before illumination, the photocurrent values of the four samples were almost zero. After the light source was turned on, the photoelectric response of SnO_2/TNRs composite (31 to 84 $\mu A \cdot cm^{-2}$) were higher compared with the unmodified TNRs film (27 $\mu A \cdot cm^{-2}$), indicating that photon-to-current conversion efficiency of SnO_2/TNRs film was outstandingly improved. Namely, more electrons can be photoexcited in this composite film under white light illumination, suggesting that the SnO_2/TNRs film might provide more effective cathodic protection for 304SS than the TNRs film. From Fig. 8a, the value order of photocurrent density is as follows: STNR-1.0 > STNR-1.5 > STNR-0.5, suggesting that the STNR-1.0 might exhibit superior PCP performance on 304SS. In addition, the SnO_2/TNRs photoanode has a stable and reproducible photoelectrochemical property during three on-off cycles of the illumination. Therefore, the SnO_2/TNRs film has an advantage for an excellent photocatalytic performance.

To assessing the PCP performances of as-prepared photoelectrodes on the steel, the materials (TNRs, STNRs-0.5, STNRs-1.0 and STNRs-1.5 films) serve as photoanode in the photo-induced OCP tests via monitoring the change of steel surface potential under white light illumination (as displayed in Fig. 8b). The result shows the corrosion

potential of bare steel is about -180 mV vs. Ag/AgCl, meanwhile, the OCP value of 304SS coupled to TNRs film shifts slightly to negative values (-320 mV vs. Ag/AgCl). Nevertheless, for SnO_2/TNRs films, the much more negative OCP value (-400 mV vs. Ag/AgCl) of the steel can be observed when this photoanode is irradiated by white light firstly. After then, the surface potential of the steel connected to SnO_2/TNRs films go on dropping slightly, and sustain finally a negative value (-350 to -420 mV vs. Ag/AgCl). As explained above, the formation of n-n heterojunction between SnO_2 and TiO_2 can improve the separation efficiency of e^-/h^+ pairs, and then more photoelectrons are immigrated to the connected steel to decrease its surface potential, resulting in superior PCP efficiency. Additionally, after cutting off the light, the OCP value of 304SS connected to TNRs film returns to the initial level before illumination (about 190 mV vs. Ag/AgCl), indicating that it can't provide valid delay protection for 304SS. Nevertheless, it is obvious that all the surface potential of the steel coupled with SnO_2/TNRs composite films are more negative than the corrosion potential of 304SS in darkness (-210 to -230 mV vs. Ag/AgCl), which can be ascribed to the effect of "electron pool". Meanwhile, the potential of 304SS coupled with STNRs-1.0 is significantly lower than that when it is coupled with pure STNRs-0.5 and STNRs-1.5 with light illumination, implying that STNRs-1.0 is optimal for anti-corrosion of 304SS. This result could be attributed to the appropriate deposition content of SnO_2 nanoparticles coordinated with the sustainability of the 1D electron transmission shortcut of the TNRs, therefore enhancing the photon-to-electron conversion efficiency

and insuring abundant generation and rapid immigration of photoelectrons. For STNRs-0.5, because of the low deposition content of SnO_2 nanoparticles, it is unsatisfactory to generate sufficient photoelectrons to the maximum extent. For STNRs-1.5, owing to the excessive coverage of SnO_2 nanoparticles onto the surface of TNRs film, the light-absorption ability is reduced, and sectional SnO_2 nanoparticles may be the recombination center of the e^-/h^+ pairs. More interestingly, the OCP value of 304SS coupled to the STNRs-1.0 composite keeps going down to a fixed state (approximately -250 mV vs. Ag/AgCl) after cutting off the light source for the second and third time. When the STNRs-1.0 film is irradiated for the first time, extra electrons was temporarily stored in SnO_2 and then released to achieve dark-state protection. These unconsumed electrons in darkness will be continued to transferred to the coupled steel when the light is provided again, resulting in more negative surface potential of 304SS. After the second on-off cycle, the dark-state OCP shift more negatively to a fixed value due to no need of more electrons to be stored. Therefore, the STNRs-1.0 film can serve as a potential photoelectrode in the PCP applications for 304SS.

The Tafel polarization curves of 304SS in the 0.5 $mol \cdot L^{-1}$ NaCl solution were also employed to evaluate the PCP efficiency of the as-prepared samples under white light illumination (Fig. 8c). It is obvious that the E_{corr} value of 304SS connected to the as-prepared sample is more negative than that of bare 304SS (-187 mV vs. Ag/AgCl), and the E_{corr} of 304SS coupled with STNRs-1.0 film exhibits the most negative value (-421 mV vs. Ag/AgCl), which is in agreement with the OCP results. This result indicate that

STNRs-1.0 film possess the higher photo-electric conversion efficiency than pure TNRs film, and more electrons are immigrated to the coupled steel under white light irradiation. It is well known that the higher I_{corr} value, the more effective anti-corrosion property will be. The I_{corr} of STNRs-1.0 is markedly higher than those of the other samples/304SS and bare 304SS, since superior solar light utilization capacity and separation efficiency of the e^-/h^+ pairs. According to the above analysis, the STNRs-1.0 composite could be supposed to display remarkable PCP efficiency for 304SS.

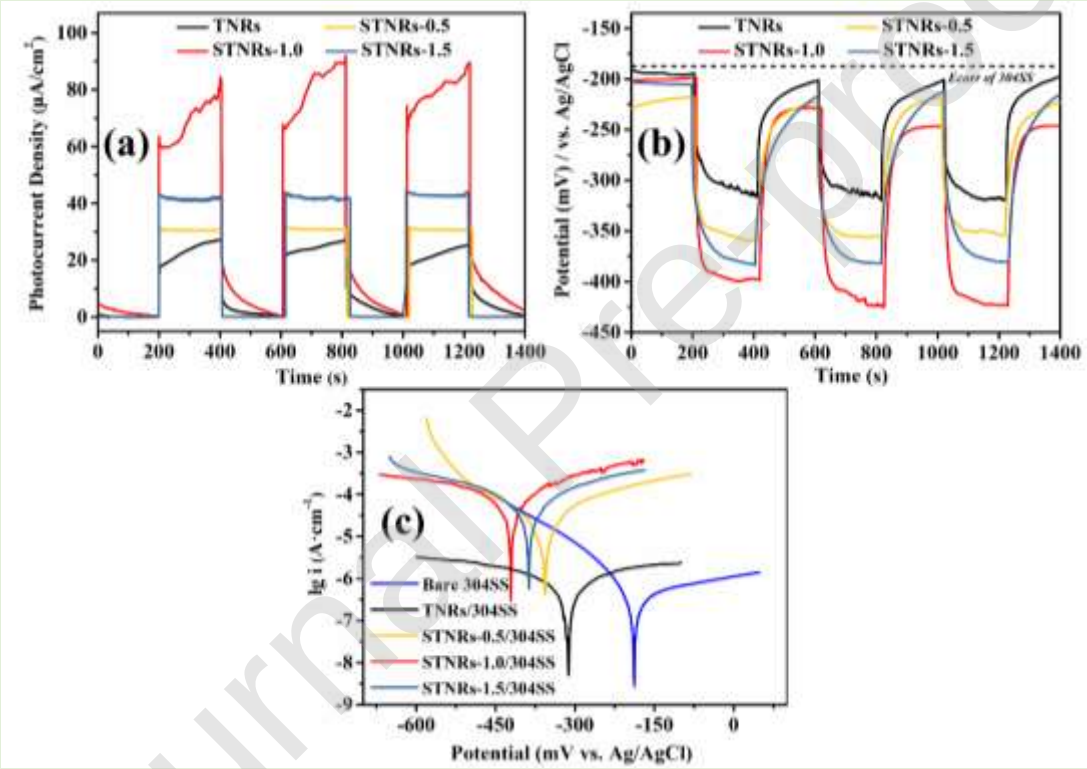

Fig. 8. (a) The photoinduced current density between the as-prepared samples and 304SS under intermittent light illumination. (b) The potential change of the 304SS electrodes coupled with the as-prepared films. Polarization curves (c) of bare 304SS, and 304SS coupled with TNRs, and SnO_2/TNRs films electrodes under illumination,

3.3 The stability evaluation of STNRs-1.0 film in PCP system of 304SS

As shown in Fig. 9a, the relationship between the illumination time of white light and the dark-state delay PCP performance of 304SS coupled with STNRs-1.0 is

investigated. After coupled with the STNRs-1.0 composite, the 304SS potential negatively shifts to around -200 mV vs. Ag/AgCl before illumination because of the galvanic effect. When provided with white light irradiation, all the potential values rapidly dropped to -440 mV vs. Ag/AgCl, which are consistent with the above results. When the STNRs-1.0 film was only irradiated with white light for 5 min, the OCP value of the 304SS recovered to its the initial potential (-200 mV vs. Ag/AgCl) after 20 min (about 0.34 h). After extending the illumination time to 30 min, the duration of the delay protection could be effectively increased to 4.71 h. However, when the illumination time was extended to 60 min further, the duration of the delay protection (about 4.92 h) is almost identical to that of the above result (illumination for 30 min). These results demonstrate that the increase of illumination time is in favor of the dark-state protection of 304SS, nevertheless, the enhancement extent of delay protection is limited and the STNRs-1.0 film can provide certain degree of delay protection even when the light source is turned off during this period.

In order to estimate the photoresponse stability of SiO_2/TNRs film in the PCP system, the OCP value changes of the 304SS coupled with STNRs-1.0 film to intermittently white light irradiation were measured (as shown in Fig. 9b). This result displays that the STNRs-1.0 film can prevent continuously and effectively 304SS from corrosion, and the OCP value (around -220 mV vs. Ag/AgCl) of 304SS is still lower for comparison with its initial value (around -200 mV vs. Ag/AgCl) and corrosion potential under 8 hours' intermittent light irradiation, displaying distinguished stability of this

composite films. The SEM image of STNRs-1.0 film measured in the above stability evolution experiment, are exhibited in Fig. 9c. It can be obviously seen that a mass of SnO_2 are still steadily anchored on the surface of TNRs film, and there isn't much mass SnO_2 to strip from the substrate. Therefore, such composite film has good potential in PCP application.

In the PCP system, the S^{2-} of the electrolyte of the photoelectrochemical cell plays an extremely key role to eliminate h^+ (equation (2)), aiming to promote the separation of photocarriers and further enhance the PCP efficiency [28]. However, the accompanying elemental sulfur (S) may deposit onto the surface of the composite film to hinder the immigration of free carrier. The XPS survey spectrum of the STNRs-1.0 film after PCP experiment is shown in Fig 9d, and there is no peaks for elemental S, which suggests that the reaction-generated elemental S forms dissolvable polysulfide ions in the solution (equation (3) and (4)) [29]. Therefore, the elemental S originated from the oxidation reaction of S^{2-} does not exist onto the surface of the electrode, and have little influence on the PCP performance.

$$S^{2-} + 2h^+ \rightarrow S \quad (2)$$

$$(x-1)S + S^{2-} \rightarrow S_x^{2-} (x = 2-5) \quad (3)$$

$$S + S_x^{2-} \rightarrow S_{x+1}^{2-} (x = 2-4) \quad (4)$$

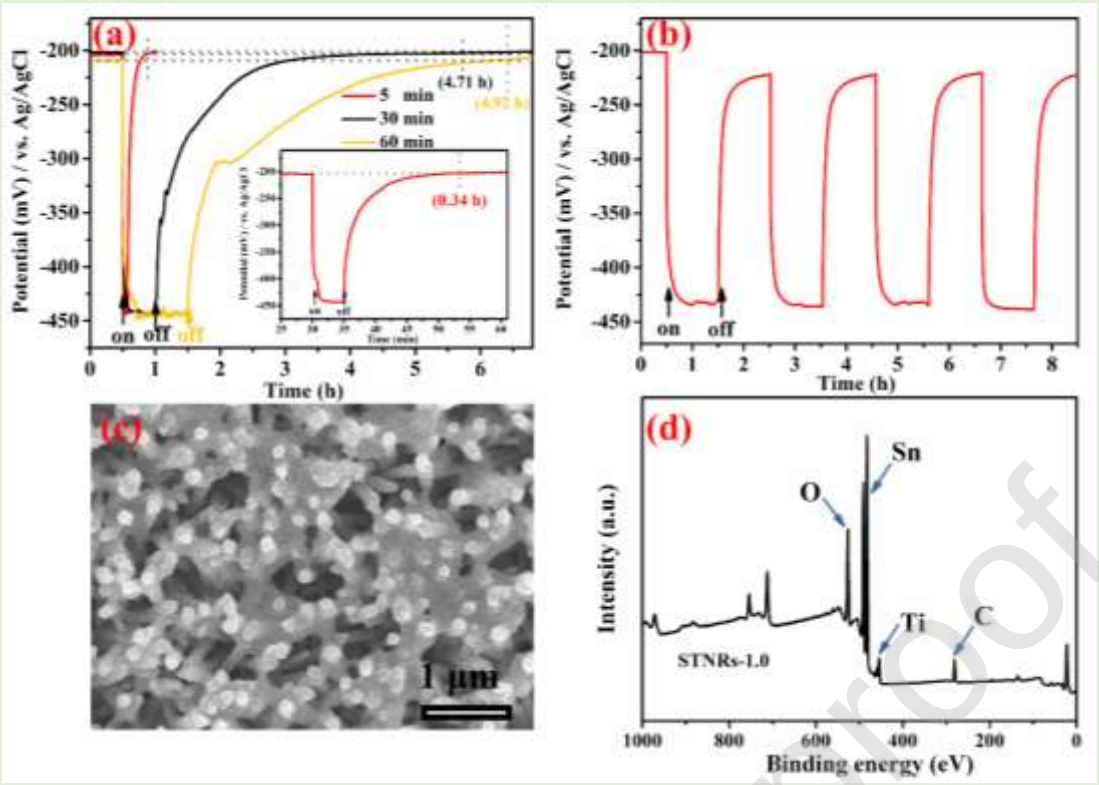

Fig. 9. (a) The potential change of the 304SS electrodes coupled with the STNRs-1.0 film under different-time intermittent visible light illumination. (b) The potential change of the 304SS electrodes coupled with the STNRs-1.0 film under 4 light on/off cycles. The SEM images (c) and the full scan survey XPS spectrum (d) of the STNRs film, which was used in the above stability evaluation experiments for 8 h under intermittent visible light illumination.

3.4 Mechanism

After evaluating the PCP performances of the TNRs and SnO_2/TNRs films, the e^-/h^+ separation and immigration mechanism for this SnO_2/TNRs composite electrode with and without white light irradiation in the PCP application for 304SS were described in Fig. 10. The band gap of SnO_2 is wider than that of rutile TiO_2, and the CB and valance band (VB) of SnO_2 can match well with those of TiO_2 [14]. When the white light illumined this composite film, the photogenerated electrons in the VB of TiO_2 and SnO_2 were photoexcited and immigrated to their CB, respectively. Meanwhile, a majority of photoelectrons were rapidly transferred to the 304SS through FTO substrate because of a lower potential (304SS) [30], resulting in that the protected steel was in the state of

thermodynamic stability. Compared with the pure TNRs photoanode, both of the photoexcited electrons of two kinds materials could immigrated to the coupled steel, leading to a better PCP performance

At the same time, sectional electrons in TiO_2 CB could be immigrated to SnO_2 CB under white light illumination, because the CB of the latter is more negative than that of the former. And the photogenerated holes assembled in TiO_2 VB in the opposite direction are vanished by S^{2-} at the photoanode/electrolyte interface. The ordered band-gap structure is favour of the separation of e^-/h^+ pairs, resulting in that more electrons of SnO_2 and TiO_2 are immigrated to the steel surface. Meanwhile, sectional electrons could be served in SnO_2 CB temporarily, due to its inherent property via a reduction reaction as follows [13, 31-33]:

$$SnO_2 + xe^- + xM^+ \rightleftharpoons M_xSnO_2 \quad (M = Na \text{ or } H,\ x = 1 \text{ or } 2)$$

with white light illumination, the electrons will be saved in SnO_2 temporarily. After cutting off the light, above reaction reverses to discharge the photoelectrons. Meanwhile, there are a small amount of OVs in the TNRs, and the energy levels of OVs have been reported to be about 1.18 eV below the CB of the rutile TiO_2 [34]. Therefore, the electron transitions from the CB of SnO_2 to the OVs levels of TiO_2 contributed to the electron transfer from SnO_2 to TiO_2 along the 1D electron shortcut. And this is the principal factor to achieving the delay protection for 304SS in the dark.

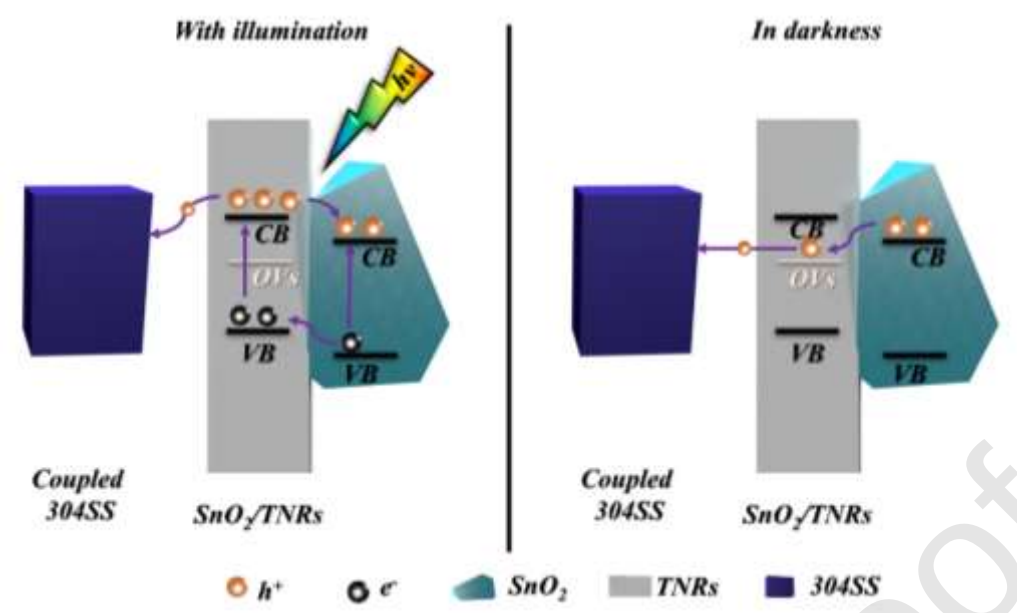

Fig. 10. The sketch of the proposed charge photogeneration and transfer mechanism in the SnO_2/TNRs film for the PCP application with and without solar light illumination.

4 Conclusion

In this research, SnO_2/TNRs composite film was successfully synthesized with enhanced PCP performances and electrons storage ability via hydrothermal treatment combined with electrodeposition method. Compared with the pure TNRs film, the SnO_2/TNRs composite film possesses superior light response ability and photoelectrochemical efficiency. The photocurrent density of this composite film is almost three times higher than that of the pure TNRs based on the deposition of SnO_2 nanoparticles. With white light irradiation, the SnO_2/TNRs film could exhibit superior cathodic protection performance for the 304SS in a 0.5 $mol \cdot L^{-1}$ NaCl solution compared with the pristine TNRs film. More importantly, the SnO_2/TNRs film could achieve the delay protection owing to the electrons storage property of SnO_2 material, even after cutting off the light. In a word, SnO_2/TNRs composite can be regarded as a potential

photoelectrode in the PCP applications for 304SS.

Author statement

Under supervision by Fan Lei, Liu Yunpeng and Feng Jiangtao, Zhang Juantao performed sample preparation and data analysis. Yang Hualong developed protection mechanisms and analysis. Wang Yuan performed sample preparation and structure fabrication. Cui Xiaohu and Wen Zhang performed characterization analysis. All authors read and contributed to the manuscript.

Conflict of interest statement

We declare that we have no financial and personal relationships with other people or organizations that can inappropriately influence our work, there is no professional or other personal interest of any nature or kind in any product, service and/or company that could be construed as influencing the position presented in, or the review of, the manuscript entitled.

Acknowledgements

The authors gratefully acknowledge the Basic Research and Strategic Reserve Technology Research Fund of China National Petroleum Corporation Project (Grant No. 2018Z-01), Shaanxi Key research and development projects, China (Grant No. 2017SF-386) and the Fundamental Research Funds for the Central Universities of China.

Reference

[1] J. Zhang, R.G. Du, Z.Q. Lin, Y.F. Zhu, Y. Guo, H.Q. Qi, L. Xu, C.J. Lin, Highly efficient CdSe/CdS co-sensitized TiO_2 nanotube films for photocathodic protection of stainless steel, Electrochim. Acta, 83 (2012) 59-64.

[2] H. Li, X. Wang, L. Zhang, B. Hou, Preparation and photocathodic protection performance of CdSe/reduced graphene oxide/TiO_2 composite, Corros. Sci. 94 (2015) 342-349.

[3] Y. Liu, C. Zhao, X. Wang, H. Xu, H. Wang, X. Zhao, J. Feng, W. Yan, Z. Ren, Preparation of PPy/TiO_2 core-shell nanorods film and its photocathodic protection for 304 stainless steel under visible light, Mater. Res. Bull. 124 (2020) 110751-110756.

[4] H. Xu, W. Liu, L. Cao, G. Su, R. Duan, Preparation of porous TiO_2/ZnO composite film and its photocathodic protection properties for 304 stainless steel, Appl. Surf. Sci., 301 (2014) 508-514.

[5] L. Xu, Y.F. Zhu, J. Hu, J. Zhang, Y.Z. Shao, R.G. Du, C.J. Lin, TiO_2 Nanotube Films Prepared by Anodization in Glycerol Solutions for Photocathodic Protection of Stainless Steel, J. Electrochem. Soc. 161 (2014) C231-C235.

[6] Y.-F. Zhu, L. Xu, J. Hu, J. Zhang, R.G. Du, C.J. Lin, Fabrication of heterostructured $SrTiO_3$/TiO_2 nanotube array films and their use in photocathodic protection of stainless steel, Electrochim. Acta 121 (2014) 361-368.

[7] S. Cui, X. Yin, Q. Yu, Y. Liu, D. Wang, F. Zhou, Polypyrrole nanowire/TiO_2 nanotube nanocomposites as photoanodes for photocathodic protection of Ti substrate and 304 stainless steel under visible light, Corros. Sci. 98 (2015) 471-477.

[8] S.S. Ge, Q.X. Zhang, X.T. Wang, H. Li, L. Zhang, Q.Y. Wei, Photocathodic protection of 304 stainless steel by MnS/TiO_2 nanotube films under simulated solar light, Surf. Coat. Technol. 283 (2015) 172-176.

[9] J. Hu, Q. Liu, H. Zhang, C.D. Chen, Y. Liang, R.G. Du, C.J. Lin, Facile ultrasonic deposition of SnO_2 nanoparticles on TiO_2 nanotube films for enhanced photoelectrochemical performances, J. Mater. Chem. A 3 (2015) 22605-22613.

[10] J. Hu, Y.F. Zhu, Q. Liu, Y.B. Gao, R.G. Du, C.J. Lin, SnO_2 Nanoparticle Films Prepared by Pulse Current Deposition for Photocathodic Protection of Stainless Steel, J. Electrochem. Soc. 162 (2015) C161-C166.

[11] H. Li, X. Wang, L. Zhang, B. Hou, CdTe and graphene co-sensitized TiO_2 nanotube array photoanodes for protection of 304SS under visible light, Nanotechnology 26 (2015) 155704-155714.

[12] W. Liu, K. Yin, F. He, Q. Ru, S. Zuo, C. Yao, A highly efficient reduced graphene oxide/SnO_2/TiO_2 composite as photoanode for photocathodic protection of 304 stainless steel, Mater. Res. Bull. 113 (2019) 6-13.

[13] J. Zhang, Z. Ur Rahman, Y. Zheng, C. Zhu, M. Tian, D. Wang, Nanoflower like SnO_2-TiO_2 nanotubes composite photoelectrode for efficient photocathodic protection of 304 stainless steel, Appl. Surf. Sci. 457 (2018) 516-521.

[14] T.H. Huy, D.P. Bui, F. Kang, Y.F. Wang, S.H. Liu, C.M. Thi, S.J. You, G.M. Chang, V.V. Pham, SnO_2/TiO_2 nanotube heterojunction: The first investigation of NO degradation by visible light-driven photocatalysis, Chemosphere 215 (2019) 323-332.

[15] Y. Zhang, Q. Lin, N. Tong, Z. Zhang, H. Zhuang, X. Zhang, W. Ying, H. Zhang, X. Wang, Simple Fabrication of SnO_2 Quantum-dot-modified TiO_2 Nanorod Arrays with High Photoelectrocatalytic Activity for Overall Water Splitting, Chemphyschem 19 (2018) 2717-2723.

[16] B. Sun, Y. Chen, L. Tao, H. Zhao, G. Zhou, Y. Xia, H. Wang, Y. Zhao, Nanorods Array of SnO_2 Quantum Dots Interspersed Multiphase TiO_2 Heterojunctions with Highly Photocatalytic Water Splitting and Self-Rechargeable Battery-Like Applications, ACS Appl. Mater. Interfaces 11

(2018) 2071-2081.

[17] Y. Li, Q. Zhang, L. Niu, J. Liu, X. Zhou, TiO_2 nanorod arrays modified with SnO_2-Sb_2O_3 nanoparticles and application in perovskite solar cell, Thin Solid Films 621 (2017) 6-11.

[18] S.V. Mohite, V.V. Ganbavle, K.Y. Rajpure, Photoelectrochemical performance and photoelectrocatalytic degradation of organic compounds using Ga:WO_3 thin films, J. Photochem. Photobiol., A 344 (2017) 56-63.

[19] Y. Liu, W. Zhang, C. Zhao, H. Wang, J. Chen, L. Yang, J. Feng, W. Yan, Study on the synthesis of poly(pyrrole methane)s with the hydroxyl in different substituent position and their selective adsorption for Pb^{2+}, Chem. Eng. J. 361 (2019) 528-537.

[20] P. Zhang, S. Zhu, Z. He, K. Wang, H. Fan, Y. Zhong, L. Chang, H. Shao, J. Wang, J. Zhang, C.N. Cao, Photochemical synthesis of SnO_2/TiO_2 composite nanotube arrays with enhanced lithium storage performance, J. Alloys Compd. 674 (2016) 1-8.

[21] H. Zhu, J. Tao, X. Dong, Preparation and Photoelectrochemical Activity of Cr-Doped TiO_2 Nanorods with Nanocavities, J. Phys. Chem. C 114 (2010) 2873-2879.

[22] P.K. Giri, B. Santara, K. Imakita, M. Fujii, Microscopic origin of lattice contraction and expansion in undoped rutile TiO_2 nanostructures, J. Phys. D-Appl. Phys. 47 (2014) 215302-215315.

[23] W. Cui, J. He, H. Wang, J. Hu, L. Liu, Y. Liang, Polyaniline hybridization promotes photo-electro-catalytic removal of organic contaminants over 3D network structure of rGH-PANI/TiO_2 hydrogel, Appl. Catal., B 232 (2018) 232-245.

[24] Q. Shi, Z. Li, L. Chen, X. Zhang, W. Han, M. Xie, J. Yang, L. Jing, Synthesis of SPR Au/$BiVO_4$ quantum dot/rutile-TiO_2 nanorod array composites as efficient visible-light photocatalysts to convert CO_2 and mechanism insight, Appl. Catal., B 244 (2019) 641-649.

[25] M.K. Singh, M.C. Mathpal, A. Agarwal, Optical properties of SnO_2 quantum dots synthesized by laser ablation in liquid, Chem. Phys. Lett. 536 (2012) 87-91.

[26] L. Zhang, Y. Li, Q. Zhang, H. Wang, Well-dispersed Pt nanocrystals on the heterostructured TiO_2/SnO_2 nanofibers and the enhanced photocatalytic properties, Appl. Surf. Sci. 319 (2014) 21-28.

[27] Y. Yang, Y.F. Cheng, Factors Affecting the Performance and Applicability of $SrTiO_3$ Photoelectrodes for Photoinduced Cathodic Protection, J. Electrochem. Soc. 164 (2017) C1067-C1075.

[28] J. Ren, B. Qian, J. Li, Z. Song, L. Hao, J. Shi, Highly efficient polypyrrole sensitized TiO_2 nanotube films for photocathodic protection of Q235 carbon steel, Corros. Sci. 111 (2016) 596-601.

[29] Anani, A. A., Electrochemical Production of Hydrogen and Sulfur by Low-Temperature Decomposition of Hydrogen Sulfide in an Aqueous Alkaline Solution, J. Electrochem. Soc. 137 (1990) 2703-2709.

[30] Q. Wei, X. Wang, X. Ning, X. Li, J. Shao, H. Li, W. Wang, Y. Huang, B. Hou, Characteristics and anticorrosion performance of WSe_2/TiO_2 nanocomposite materials for 304 stainless steel, Surf. Coat. Technol. 352 (2018) 26-32.

[31] R. Subasri, T. Shinohara, K. Mori, TiO_2-Based Photoanodes for Cathodic Protection of Copper, J. Electrochem. Soc. 152 (2005) B105-B110.

[32] Raghavan, Subasri, Tadashi, Shinohara, Kazuhiko, Mori, Modified TiO_2 coatings for cathodic protection applications, Sci. Technol. Adv. Mater. 6 (2005) 507-507.

[33] H. Li, X. Wang, Y. Liu, B. Hou, Ag and SnO_2 co-sensitized TiO_2 photoanodes for protection of 304SS under visible light, Corros. Sci. 82 (2014) 145-153.

[34] N. Wei, Y. Liu, M. Feng, Z. Li, S. Chen, Y. Zheng, D. Wang, Controllable TiO_2 core-shell phase heterojunction for efficient photoelectrochemical water splitting under solar light, Appl. Catal., B 244 (2019) 519-528.